PERGAMON

International Journal of Solids and Structures 37 (2000) 4005–4031

INTERNATIONAL JOURNAL OF SOLIDS and STRUCTURES

www.elsevier.com/locate/ijsolstr

Application of ALE finite elements method to a lubricated friction model in sheet metal forming

F. Martinet [1], P. Chabrand*

Laboratoire de Mécanique et d'Acoustique — C.N.R.S., 31, Chemin Joseph Aiguier, 13402 Marseille Cedex 20, France

Received 19 February 1999; in revised form 13 July 1999

Abstract

An Arbitrary Lagrangian Eulerian (ALE) formulation involving the use of an operator splitting procedure is presented. In solid mechanics applications, ALE formulation is employed to overcome mesh distorsion problems in finite deformation. Here, we present a new application to fluid/structure interaction problems: determining the film thickness h in lubricated contact analysis using a method of characteristic in the framework of a finite element method. Hydrodynamic and elastohydrodynamic lubrication regimens are analyzed using an averaged Reynolds equation. The friction stress is then expressed in terms of lubricant parameters such as the film thickness and viscosity and forming process parameters such as the pressure, forming speed and surface roughness. The efficiency of the method is illustrated in the case of three examples. The first one involves the ALE formulation developed here in sheet metal forming and the others are applications to lubricated contact analysis.

Keywords: Arbitrary Lagrangian Eulerian formulation; Contact; Finite element; Friction; Lubrication; Sheet metal forming

1. Introduction

In studies on sheet metal forming processes, large deformations have to be taken into account. When finite element modeling approaches are used, this requires paying particular attention to the mesh characteristics. In structures subjected to heavy loading, the components are liable to be deformed, and this can affect the quality of the solution.

In order to avoid having to perform complex mesh refinement procedures, which considerably lengthen the calculation time, an Arbitrary Lagrangian Eulerian (ALE) formulation was used here with

* Corresponding author. Fax: +33-4-91-16-44-81.
E-mail address: chabrand@lma.cnrs-mrs.fr (P. Chabrand).
[1] Present address: Samtech, Parc d'Activités du Pas du Lac, 6 avenue Ampére, 78180 Montigny le Bretonneux.

0020-7683/00/$ - see front matter
PII: S0020-7683(99)00205-X

a view to controlling the mesh characteristics. For this purpose, an additional set of unknowns relating to an independent referential domains introduced (Hugues et al., 1981), corresponding to the displacements of the mesh nodes, but independent a priori of the displacement of the material particles.

This method was first developed in fluid mechanics and has been successfully applied in Refs. (Donéa, 1978; Belytschko and Kennedy, 1978) to fluid/structure coupling problems where the fluid meshing in the flow is Eulerian and links up with the meshing of the structure interfaces.

An ALE formulation has been implemented in a solid mechanics finite element software program. An operator splitting technique makes it possible to divide the computations into two distinct steps: a Lagrangian step and an Eulerian one.

Here, we investigate a new application of the ALE approach to fluid/structure coupling problems. It is proposed to focus in particular on the effects of the lubricant on the friction occurring between the tool and the sheet metal.

Our aim here was to develop a friction model depending on local contact conditions. The friction coefficient, which was determined experimentally, depends on the microscopic contact parameters, particularly on the pressure, the velocity and in some cases on the lubricant viscosity. Tribologists have classically proceeded by drawing Stribeck curves giving the evolution of the friction coefficient versus the Sommerfield parameter $H = (\eta v)/P$, where η is the lubricant viscosity, v the velocity and P the pressure. On these graphs, the strong dependence of μ on these parameters can be observed. At low values of H, μ reaches is largest values, corresponding to dry friction. When H is large, the opposite occurs, and μ reaches its lowest values, which correspond to a completely film lubricated friction. In the mixed regimen, mid-way between these two states, the value of the friction coeffient decreases very fast.

Numerical models developed by Carleer (1997) and Chabrand and Chertier (1996) in the framework of a finite element formulation, working on the local contact node scale, have yielded a law of evolution for the macroscopically identified friction coefficient. The friction coefficient depends on the local contact variables, the sliding velocity and the normal contact force. In Ref. (Chabrand et al., 1998), it was established that in the modeling of a classical tribological experiment with flat dies, stick/slip phenomena can be observed, depending on the microscopic pressure and velocity. The frequencies of these oscillatory phenomena were found to be in the audible frequency range. The point of this study is, therefore, to illustrate the effects of local changes in the friction coefficient.

The contact between two metal surfaces also depends on the micro-geometry at the surfaces of the bodies, which is not properly accounted for in a macroscopic friction analysis. In particular, it has been observed (Ike and Makinouchi, 1990) in the unlubricated case that microscopic asperities can lead, during the loading of the test-piece, to the occurrence of plastic deformations, which develop towards the core. These plastic deformations are not susceptible to macroscopic analysis, with which only elastic deformations are observed in the case of flat dies.

In addition, the shearing of these asperities can increase the friction locally. The association of these two phenomena (the flattening and shearing of microscopic asperities) can then affect the morphology of the deformation, damage the surface finish and lead to the tearing of the coating of coated sheet metal pieces.

It seemed necessary to develop an improved friction model for dealing with these two classes of parameters, i.e., those which are external to the interface, the pressure and the velocity, and those which are internal, the surfaces roughness, and if necessary, a third body, the lubricant. A friction model was developed in the framework of hydrodynamic and elastohydrodynamic regimens, based on the model described in Ref. (Patir and Cheng, 1978) and on a procedure introduced in Ref. (Wilson and Sheu, 1988), whereby the determination of the thickness of the film, calculated by using a Eulerian characteristics method, is linked using ALE formulation to the deformations undergone by the structure, expressed in Lagrangian terms. In the first part of the paper, we present the ALE formulation which has been developed and integrated into the finite elastoplastic part of our software program. The validity of

this formulation was confirmed in the case of a coining test. The second part deals with the lubricated friction model. The coupling between solid and fluid analysis is illustrated in the case of two sheet metal forming examples.

2. General theory of ALE formulation

2.1. Why an ALE formulation?

We consider a solid S included in R^3. The set of particle positions composing S is called its configuration. In finite deformation, two different configurations have to be distinguished. The initial configuration (material domain) is denoted by C_0, and the current configuration (spatial domain) by C_t (Fig. 1).

In solids mechanics, in order to track the material particle, the Lagrangian formulation is generally used to describe the motion of S from C_0 to C_t via a mapping:

$$\varphi: C_0 \times]0, T[\rightarrow C_t$$

where $]0, T[$ denotes an open time interval included in R.

The particle which occupies the spatial point M_0 at position $X = (X_1, X_2, X_3)$ in C_0 occupies the spatial point M at position $x = (x_1, x_2, x_3)$ in C_t, with $\varphi = (X, t)$.

In the finite element discretization, the initial configuration is covered with a mesh. A node is then associated with the same material particle throughout the deformation process. The mesh is then deformed along with the body. However, this method suffers from numerical difficulties when the elements are too severely distorted or when complex contact conditions have to be dealt with.

One alternative consists of choosing a fixed mesh. This formulation, called the Eulerian formulation, is mostly used in fluid mechanics, where the current time step is the only one studied. However, the migration of material particles on the fixed mesh brings about convective effects and in finite deformation, it is still difficult to treat the free surface.

In order to overcome these difficulties, an ALE formulation is employed which combines the advantages of the two procedures described above. The mesh is deformed as in Lagrangian formulation, but independently from the body, as in Eulerian formulation.

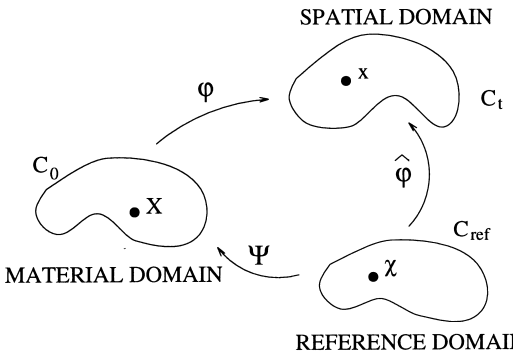

Fig. 1. Diagrams of domains and mappings for ALE formulation.

Table 1
Material and referential description

	Material	Referential
Motion	$x = \varphi(X, t)$	$x = \hat{\varphi}(\chi, t)$
Displacement	$u = x - X$	$\hat{u} = x - \chi$
Velocity	$v = \dfrac{\mathrm{d}u}{\mathrm{d}t} = \left.\dfrac{\partial x}{\partial t}\right\|_X$	$\hat{v} = \dfrac{\mathrm{d}\hat{u}}{\mathrm{d}t} = \left.\dfrac{\partial x}{\partial t}\right\|_\chi$

2.2. Referential configuration

The general theory of ALE formulation is based on choosing a third configuration C_{ref}, called the reference configuration, which is independent of both the material (C_0) and spatial (C_t) ones. The referential coordinate is denoted χ. We assume that the reference domain is related to the spatial one by the mapping $\hat{\varphi}$:

$$\hat{\varphi}: C_{\mathrm{ref}} \times]0, T[\rightarrow C_t$$

Every point M in C_t is the image of a unique point $\hat{M}$ in C_{ref} (through $\hat{\varphi}$), and of a unique point M_0 in C_0 (through φ). The spatial coordinates of M satisfy $x = \hat{\varphi}(\chi, t) = \varphi(X, t)$. Table 1 gives the motion, displacement and velocity in the initial and referential configurations.

Comment. In addition, we assume that φ and $\hat{\varphi}$ are sufficiently smooth functions of each argument. Consequently, we can define a third mapping between C_{ref} and C_0 as $\Psi = \varphi^{-1} \circ \hat{\varphi}$.

In finite element numerical discretization, as in Lagrangian formulation, the referential configuration is covered with a mesh. The particles composing C_{ref} are, therefore, associated with mesh nodes. Each node is also associated with one and only one material particle in the initial configuration C_0 using Ψ.

During the deformation process, the material particle moves with φ, whereas the mesh node moves with $\hat{\varphi}$. Consequently, in the current configuration C_t, the node mesh is associated with a different material particle than in C_0. Based on these considerations, $\hat{\varphi}$ describes the movement of a grid. For this reason, $\hat{u}$ and $\hat{v}$ are called the grid displacement and the grid velocity, respectively. Depending on the formulation used, $\hat{u}$ and $\hat{v}$ have the following values:

- In Lagrangian formulation, C_{ref} is combined with C_0 (i.e. $\varphi = \hat{\varphi}$) and the displacement and velocity of the grid are equal to those of the associated material particles.
- In Eulerian formulation, the mesh remains fixed. C_{ref} is combined with C_t (i.e. $\forall t \in]0, T[\hat{\varphi} = Id$) and the grid displacement and velocity are zero.
- In ALE formulation, a mesh point moves ($\hat{u} \neq 0$) but does not remain associated with the same material particle ($\hat{u} \neq u$).

As in the Eulerian description, the difference between material and mesh displacement has convective effects. It is, therefore, necessary to introduce a convective velocity denoted $c = v - \hat{v}$, which is the relative velocity between the material and the mesh.

3. Basic equations in ALE formulation

The conservation laws in the ALE formulation are determined from their expression written on the current configuration using a referential derivative presented below.

3.1. Time derivative relation

In Lagrangian descriptions, the balance laws require time derivatives of functions depending on material coordinates X. Taking a function f defined on the current configuration C_t (according to the spatial coordinates x), we can write:

$$f(x, t) = f\big(\varphi(X, t), t\big) = \tilde{f}(X, t) \tag{1}$$

Using the classical material time derivative defined by $\dot{f} = (\partial\tilde{f}/\partial t)|_X$, the following spatial time derivative is obtained:

$$\dot{f} = \left.\frac{\partial f}{\partial t}\right|_x + v \cdot \nabla f \tag{2}$$

where v is the material velocity and ∇f the tensor gradient f.

In ALE formulation, since χ is the computational reference coordinate, it is convenient to express f in terms of χ and t:

$$f(x, t) = f\big(\hat{\varphi}(\chi, t), t\big) = \hat{f}(\chi, t) \tag{3}$$

We define a referential derivative $\mathring{f}$ as:

$$\mathring{f} = \left.\frac{\partial \hat{f}}{\partial t}\right|_\chi = \left.\frac{\partial f}{\partial t}\right|_x + \hat{v} \cdot \nabla f \tag{4}$$

which can be related to the material derivative by:

$$\dot{f} = \mathring{f} + c\nabla f \tag{5}$$

with the convective velocity c.

3.2. Conservation laws in ALE formulation

3.2.1. Mass conservation equation

Let the volume $\mathrm{d}v$ in C_t be the image of a volume $\mathrm{d}V$ in C_0, related by:

$$\mathrm{d}v = J\,\mathrm{d}V \tag{6}$$

where $J = \det \mathbb{F}$ and $\mathbb{F} = \operatorname{grad} \varphi$.

Writting ρ for the mass density of $\mathrm{d}v$ and ρ_0 for the mass density of $\mathrm{d}V$, the classical mass conservation equation becomes:

$$J\rho = \rho_0 \tag{7}$$

The derivative form of this equation gives the material conservation law of mass:

$$\dot{\rho} = -\rho \operatorname{div} v \tag{8}$$

Using an ALE formulation, the corresponding referential equation of Eq. (8) is obtained from relation (5):

$$\mathring{\rho} = -\rho \operatorname{div} v - c\nabla\rho \tag{9}$$

3.2.2. Momentum and energy conservation equations

The referential form of momentum and energy conservation equations is determined using a similar approach to that used for the continuity equation. The momentum conservation equation is written as follows:

$$\rho\mathring{v} = \operatorname{div}\sigma + f^{\mathrm{v}} - \rho c\nabla v \tag{10}$$

where f^{v} stands for the volumic force density and σ stands for the Cauchy stress tensor. Taking W to be the internal rate of energy, then the conservation equation is:

$$\mathring{W} = \sigma \cdot \nabla v + \rho r - \operatorname{div} q - c\nabla W \tag{11}$$

where r is the volumic rate of heat transfer and q the heat flux.

Comment. The convective additional term in each equation makes ALE equations much more difficult to solve numerically than Lagrangian ones (where $\forall f \quad \mathring{f} = \dot{f}$ and $c = 0$).

3.3. Equations governing the continuum

3.3.1. Equilibrium

We take a quasi-static approach neglecting the inertial effects in finite deformation, which is appropriate for forming processes such as those studied in the present investigation. The equation of motion is given by the momentum conservation equation (10), in which the additional convective term disappears in the first step:

$$\operatorname{div}\sigma + f^{\mathrm{v}} = 0 \quad \text{in } C_t \tag{12}$$

In addition, we use the classical boundary condition (without contact):

$$f^{\mathrm{s}} = \sigma \cdot n \tag{13}$$

on the part of Γ called Γ_f, which is subjected to surface force density f^{s} and

$$u = \bar{u} \tag{14}$$

on the part of Γ called Γ_u, which is subjected to the prescribed displacement (with the usual boundary properties $\Gamma = \Gamma_f \cup \Gamma_u$ and $\Gamma_f \cap \Gamma_u = \varnothing$).

3.3.2. Constitutive equation

In the present study, we deal with an elastoplastic behavior based on the multiplicative decomposition of the gradient deformation $\mathbb{F} = \mathbb{F}^{\mathrm{e}} \cdot \mathbb{F}^{\mathrm{p}}$ into its elastic and plastic parts, as proposed by Lee (1969). The behavior between the intermediate configuration (defined by $\mathbb{F}^{\mathrm{e}}$) and the current one is characterized by

a hyperelastic response. The constitutive law of the material is determined from the free energy density function W, which is an isotropic function of the elastic part of the left Cauchy–Green strain tensor $b^{e} = \mathbb{F}^{e}\mathbb{F}^{e^{T}}$ and of the equivalent plastic strain $\bar{\varepsilon}_{p}$. Neglecting superscript e, the Kirchhoff stress tensor can then be expressed as follows in the current configuration (see, for example, Sidoroff, 1982):

$$\tau_{ij} = 2b_{ij}\left(\frac{\partial W}{\partial b}\right)_{ij} \tag{15}$$

or in the initial configuration:

$$\tau_{ij} = \frac{2}{J}\mathbb{F}_{iI}\mathbb{F}_{jJ}\left(\frac{\partial W}{\partial C}\right)_{IJ} \tag{16}$$

where $C = \mathbb{F}^{t}\mathbb{F}$ is the right Cauchy–Green tensor.

The plastic flow rule is described by a classical von-Mises criterion with isotropic hardening:

$$f(\tau, \bar{\varepsilon}_{p}) = \sqrt{\frac{3}{2}\mathrm{dev}(\tau):\mathrm{dev}(\tau)} - A_{0}(\bar{\varepsilon}_{p}) \leq 0 \tag{17}$$

where $A_0(\bar{\varepsilon}_p)$ stands for the thermodynamic force associated with the hardening variable $\bar{\varepsilon}_p$.

The evolution of the plastic strain rate d^p and that of the internal hardening variable are written for $\lambda \geq 0$ as:

$$\left.\begin{aligned} d^{p} &= \lambda\left(\frac{\partial f}{\partial \tau}\right) = \lambda\sqrt{\frac{3}{2}}\frac{s}{\|s\|} \\ \dot{\bar{\varepsilon}}_{p} &= -\lambda\frac{\partial f}{\partial A_{0}} = \lambda = \sqrt{\frac{2}{3}d^{p}:d^{p}} \end{aligned}\right\} \lambda \leq 0\ f(\tau, \bar{\varepsilon}_{p}) 0 \leq\ \lambda \cdot f = 0 \tag{18}$$

The energy density used here is presented in Ref. (Simo and Miehe, 1992) and written:

$$W = \frac{K}{2}\left[\frac{1}{2}(J^{2} - 1) - \ln J\right] + \frac{1}{2}\mu(I_{b} - 3) \tag{19}$$

where μ is the second Lame coefficient, K the bulk modulus and I_b the first invariant of b.

3.3.3. Principle of virtual works

We introduce a convective referential system into C_{ref}. In the referential configuration, the convective referential system ($\tilde{G}_1$, $\tilde{G}_2$, $\tilde{G}_3$) is neither fixed (Cartesian referential system) nor associated with material particles (material referential system). This choice is justified by the principle of ALE formulations, in which the material deformation is described without remaining associated with the same particle. We denote (g_1, g_2, g_3) in the current configuration and (G_1, G_2, G_3) in the initial configuration the images of this convective referential system. The metric tensor associated with the covariant convective basis (g_1, g_2, g_3) in C_t is denoted by m:

$$m = m_{ab}g^{a} \otimes g^{b} \quad \text{where } m_{ab} = g_{a} \cdot g_{b}$$

The equilibrium equations (12)–(14) lead to the principle of virtual work. Let η be the kinematically admissible variation of φ defined on C_t.

The spatial principle of virtual works is given by:

$$G(\varphi,\eta)=\int_{C_t}\sigma_{ij}\left(\nabla_m^{cs}\eta\right)_{ij}\,\mathrm{d}\Omega_t+\left(-\int_{C_t}f_i^{\mathrm{v}}\eta_i\,\mathrm{d}\Omega_t-\int_{\Gamma_t{}^f}f_i^{\mathrm{s}}\eta_i\,\mathrm{d}\Gamma_t\right)=0 \tag{20}$$

where $\nabla_m^{cs}\eta$ is the symmetric covariant gradient of η associated with the metric m:

$$\left(\nabla_m^{cs}\eta\right)_{ab}=\eta(a,b)=\frac{\eta^c\big|_a m_{cb}+\eta^c\big|_b m_{ca}}{2}$$

Noting $\eta\circ\varphi$ the material version of the kinematically admissible variation (which is also denoted η below to simplify the writing), the material form of the principle of virtual works is expressed as follows:

$$G(\varphi,\eta)=\int_{C_0}2F_{iI}F_{jJ}\left(\frac{\partial W}{\partial C}\right)_{IJ}\left(\nabla_m^{cs}\eta\right)_{ij}\,\mathrm{d}\Omega_0-\int_{C_0}{}^0f_I^{\mathrm{v}}\eta_I\,\mathrm{d}\Omega_0-\int_{\Gamma_0{}^f}{}^0f_I^{\mathrm{s}}\eta_I\,\mathrm{d}\Gamma_0=0 \tag{21}$$

where ${}^0f$ stands for the force densities transported onto C_0.

The linearization of G in the ALE description (i.e. involving variable χ) requires introducing into the virtual work principle the mappings $\hat{\varphi}$ and ψ instead of φ:

$$G(\varphi,\eta)=G\left(\hat{\varphi},\psi,\eta\right)=0 \tag{22}$$

Comment. Although there is no convective term in Eq. (20) or (21), the particularity of ALE formulation (i.e. C_{ref} being independent of C_0) shows up in this linearization. In fact, the only unknown φ in the classical Lagrangian formulation is replaced by the two unknowns $\hat{\varphi}$ and ψ.

The numerical solution of this non linear variational equation is obtained with an incremental Newton–Raphson scheme. Let w and U be the kinematically admissible variation of $\hat{\varphi}$ and ψ, respectively. Taking the referential configuration, we use $w\circ\hat{\varphi}$ and $U\circ\psi$. The first order Taylor development leads to:

$$G\left(\hat{\varphi}+w\circ\hat{\varphi},\psi+U\circ\psi,\eta\right)\cong G\left(\hat{\varphi},\psi,\eta\right)+D_{\hat{\varphi}}Gw\circ\hat{\varphi}+D_{\psi}GU\circ\psi=0 \tag{23}$$

where $D_{\hat{\varphi}}Gw\circ\hat{\varphi}$ (resp. $D_{\psi}GU\circ\psi$) is the Fréchet derivative of $G(\hat{\varphi},\psi,\eta)$ with respect to $\hat{\varphi}$ (resp. ψ).

In the first Fréchet derivative $D_{\hat{\varphi}}Gw\circ\hat{\varphi}$, where all the expressions written for the initial configuration are independent of $\hat{\varphi}$, we obtained:

$$D_{\hat{\varphi}}Gw\circ\hat{\varphi}=\int_{C_0}K_1^{abcd}\left(\nabla_m^{cs}w\right)_{cd}\left(\nabla_m^{cs}\eta\right)_{ab}+\tau_{ab}\eta^c\big|_a w^b\big|_d m_{cd}\,\mathrm{d}\Omega_0 \tag{24}$$

whereas a difficulty arising in the calculation of $D_{\psi}GU\circ\psi$ is that the initial configuration depends on ψ and the Fréchet derivative of C_0 and Γ_0:

$$\begin{aligned}D_{\psi}GU\circ\Psi=&\int_{C_0}\Big(-K_2^{abcd}(\nabla^{\#s}U)_{cd}\left(\nabla_m^{cs}\eta\right)_{ab}-2\tau_{ab}U^{\#c}\big|_b\left(\nabla_m^{cs}\eta\right)_{ac}+\tau_{ab}U^{A}\big|_A\left(\nabla_m^{cs}\eta\right)_{ab}\Big)\,\mathrm{d}\Omega_0\\&+D_{\Psi}G_{\mathrm{ext}}U\circ\psi\end{aligned} \tag{25}$$

We denote $U^{\#a}|_b=U^A|_B\mathbb{F}_A^a\mathbb{F}_b^{B-1}$ the "push forward" of the covariant gradient of U in C_0 and $(\nabla^{\#s}U)_{cd}$

$= (1/2)(U^{\#c}|_a m_{cb} + U^{\#c}|_b m_{ca})$ its symmetrical expression. In Eqs. (24) and (25), K_1^{abcd} and K_2^{abcd} are fourth-order tensors given in Ref. (Yamada and Kikuchi, 1993).

G_{ext} is the work of external forces in Eq. (21) and its Fréchet derivative with respect to $\hat{\varphi}$ is equal to zero, but that with respect to Ψ leads to:

$$D_\Psi G_{\text{ext}} U \circ \Psi = -\int_{C_0} \left({}^0f^{\text{v}}_a \eta^a U^A|_A + {}^0f^{\text{v}}_{a,\,A}\, \eta^a U^A \right) \mathrm{d}\Omega_0$$

$$-\int_{\Gamma_0^f} \left({}^0f^{s}_a\, \eta^a \left(U^A|_A - U^A|_C N_A N_B M^{BC} \right) + {}^0f^{\text{s}}_{a,\,A}\, \eta^a U^A \right) \mathrm{d}\Gamma_0 \tag{26}$$

where ${}^0f^{\text{v}}_a$, $A = (\partial {}^0f^{\text{v}}_a)/(\partial X^A)$ and N is the exterior normal unit vector to Γ_0 and M the metric tensor associated with the initial configuration.

4. Numerical integration

4.1. Finite element discretization

The reference configuration is meshed with isoparametric finite elements. The material and spatial coordinates X and x are expressed in terms of the reference coordinates using the classical shape functions N^α:

$$X_I = \sum_{\alpha=1}^{nel} N^\alpha(\chi) X_I^\alpha \quad \text{and} \quad x_i = \sum_{\alpha=1}^{nel} N^\alpha(\chi) x_i^\alpha \tag{27}$$

where *nel* is the number of nodes per element. The finite element discretization of the linearized principal of virtual work leads to a tensor equation:

$$K_1 U + K_2 w = F \tag{28}$$

where F is the residual equilibrium vector and K_1 (resp. K_2) is the matrix form of the fourth-order tensor introduced above. Explicit forms of these matrices can be found in Ref. (Yamada and Kikuchi, 1993).

If U and w are unknown (i.e. fully coupled ALE method), the linear system is rectangular and does not have a unique solution. Scheurs et al. (1986) have solved this fully coupled system of equations by taking a virtually elastic body to control the mesh distorsions. Another way of overcoming this numerical difficulty is to introduce equations for computing the mesh displacement, and some authors have used fluid mechanics equations based on streamline techniques (see, for example, Belytschko and Kennedy, 1978; Hugues et al., 1981; Liu et al., 1988; Liu et al., 1986).

In the present study, in order to implement the ALE formulation in an existing Lagrangian code, we adopt another approach. At every time step, an operator splitting technique is used to eliminate half of the unknowns (see, for example, Benson, 1989; Donéa et al., 1982; Huetink and van der Lugt, 1990; Lugt et al., 1993; Ponthot, 1995; Gaston et al., 1996; Potapov and Jacquart, 1996). This technique is analogous to the predictor corrector algorithm used in the numerical integration of the constitutive equations:

- A Lagrangian step is first performed in which the mesh moves with the material.
- The Eulerian step consists of two parts:

- The nodal pattern has to be defined in order to create a new mesh under qualitative or quantitative criteria.
- The solution variables have to be remapped from the former mesh to the present one.

The Lagrangian step is a classical Lagrangian calculation, corresponding to choosing $\psi = Id$ (i.e. $U = 0$) that corresponds to $\varphi = \hat{\varphi}$. The advantage here is that the method can be easily implemented in a Lagrangian code.

4.2. Eulerian step

4.2.1. Remeshing the structure

The first part of the Eulerian step consists of remeshing the structure based on qualitative (element shape) or quantitative (mesh refinement on high strain location) criteria. However, contrary to the classical remeshing techniques, the remeshing is performed here at every time step and the topology of the initial mesh is preserved: remeshing is done at constant numbers of elements. Due to the bijective properties of the mapping $\hat{\varphi}$, one point in C_{ref} has to correspond to a single point in C_t. This condition ensures that the boundaries of the new mesh and those of the mesh obtained at the end of the Lagrangian step coincide. The remeshing is then started by repositioning the nodes of the boundary called the master lines. A transfinite mapping method proposed by Haber et al. (1981) is then used to generate the internal mesh.

To account for complex geometries, the structure is divided at the beginning of the process into regions called macroregions bounded by master lines, where the nodes are first repositioned.

4.2.2. Transport step

The second part of the Eulerian step is dedicated to remapping the unknowns involved in the problems. Hyperelastic constitutive law requires the transport of the left Cauchy–Green tensor b, and the elastoplastic response requires that of the equivalent plastic deformation $\bar{\varepsilon}_{\text{p}}$.

As remeshing is carried out at each time step with a constant number of Gauss points, the distance between the non-remeshed and remeshed integration points is small. According to these properties, a first order Taylor formula gives a sufficently accurate relation between f^{ngp}, the unknown value (i.e. at new Gauss point) and f^{lgp}, the value obtained at the Gauss point prior to the remeshing (i.e. at the lagrangian step Gauss point) (Ponthot, 1995):

$$f^{\text{ngp}} = f^{\text{lgp}} + dpg(\nabla f)^{\text{lgp}} \tag{29}$$

where dpg is the distance between the former and present integration points.

To determine $(\nabla f)^{\text{lgp}}$ (gradient value of f at material Gauss point), we have to construct a continum field from the local value of f. For this purpose, we use the nodal interpolation:

$$f^{\text{lgp}}(\xi_\alpha, \theta_\alpha) = N^i(\xi_\alpha, \theta_\alpha) f_i^{\text{ln}} \quad \alpha \in [1, nel] \tag{30}$$

where f_i^{ln} is the unknown nodal value and $N^i(\xi_\alpha, \theta_\alpha)$ the value of the shape function at the Gauss points. Solving Eq. (30) makes it possible to determine the nodal value f_i^{ln} and leads to a local least square smoothing matrix which is identical to that obtained by Hinton and Campbell (1974).

The originality of the present method is that it provides a choice between two remapping methods. The first one involves transporting the values between Gauss point locations in the initial configuration C_0 (Fig. 2):

- At every *non* remeshed element, assuming that Gauss points remain in the same element, we

determine the isoparametric coordinates of the new integration points (Step (1)).

- During the Lagrangian step, the isoparametric coordinates remain the same as in the initial configuration. Using the relation (29), b and $\bar{\varepsilon}_p$ are transported to the new Gauss point location in the initial configuration (Step (2)).
- In order to check the equilibrium in the new mesh, we compute the internal variables along a material path from the initial configuration to the current deformed one (Step (3)).

The second method consists of directly remapping the internal variables (i.e. those between the mesh obtained at the end of the Lagrangian step and the current one, see Fig. 3). It might then be necessary to check the equilibrium and elasticity criteria on the new mesh. However, the transport operations are carried out between very closely neighbouring points, and any lack of equilibrium can be overcome after some iterations during the next time step.

5. Simulating a coining process

The above procedure was applied to the numerical simulation of a coining process. An initially rectangular work-piece is crushed by a rigid tool with a prescribed vertical displacement. The geometrical and loading conditions are given in Fig. 4. The material is elastoplastic with linear isotropic hardening (see Table 2). The contact area is assumed to be frictionless.

Using a classical Lagrangian formulation with a very simple discretization (24 mixed quadrangular elements: Q4P0) procedure leads at the end of the calculation to a reduction of about 25% in height. This is due to the severe contact conditions around the tool edge. In ALE formulation, this problem can be overcome with an adaptive mesh.

The work-piece is divided into two macroregions (Fig. 4):

- Macroregion I (under the tool) is taken to be Eulerian. Master lines 1, 2, 5 are updated Eulerian: the nodal coordinate in the vertical direction is given by the tool displacement and in the horizontal direction, it remains the same. Master line 4 is purely Eulerian (no displacement).
- Macroregion II (with a free surface) is taken to be ALE. Master lines 3 and 7 are remeshed with a constant element size. Master line 6 is a mirror image of master line 7 (same coordinate in the horizontal direction and 0 in the vertical direction).

The vertical positions of the nodes are given by the position of the tool in order to ensure that the size of the elements is constant. Material particles flow out from macroregion I to macroregion II.

Fig. 5 shows the deformed mesh obtained after a 30% height reduction, using the ALE formulation.

The effective plastic strain patterns are presented in Figs. 6 and 7 using the two remapping methods after a 30% height reduction.

As we can see, the choice of configuration made when transferring the data does not affect the results, except that the calculations are made with 31 increments and 137 iterations when remapping onto the initial configuration and with 31 increments and 140 iterations onto the current configuration. This difference is due to the structural equilibrium iterations necessary in the case of C_t remapping. We, therefore, use the C_0 remapping technique.

In order to compare these results with those of a classical Lagrangian formulation, we used the more refined mesh with 1650 elements (1280 under the tool) shown in Fig. 8. The deformed mesh is shown in Fig. 9 after a height reduction of 30%. The calculation was carried out with 191 increments and more than 300 iterations!

In conclusion, the ALE formulation developed here was introduced into a Lagrangian computation code, in order to treat problems associated with mesh distortions. Modeling the coining process using a

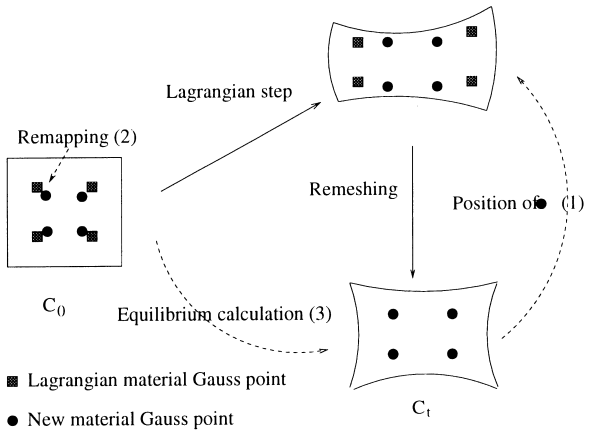

Fig. 2. Remapping on the initial configuration (for one element).

coarse mesh gives comparable results to those obtained with a very fine mesh in Lagrangian formulation.

6. Low friction for lubricated contact

Successful metal forming operations depend on process parameters such as the contact pressure and forming speed and on material parameters such as the material properties of the work-piece and the surface properties of the tool and work-piece. In addition, with these parameters, the lubrication is an important factor in the process: appropriate lubrication reduces the friction and prevents wear and tear in both the workpiece and the tool.

Nevertheless, in numerical simulation, the focus has been on the behavior of the structure and only simple friction laws (the Coulomb law with a constant coefficient is the most commonly used) have been introduced up to now.

Here, we present a friction model corresponding to the shearing of a lubricant film and depending on

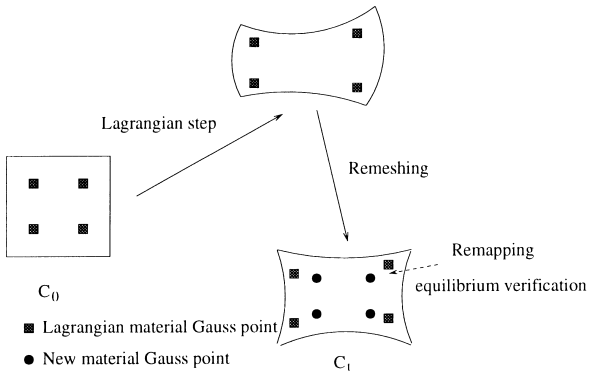

Fig. 3. Remapping the current configuration.

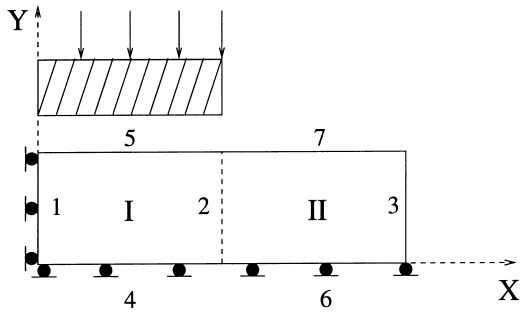

Fig. 4. Geometry of coining process.

internal interface parameters such as the surface roughness, the viscosity and the thickness of the lubricant film and on external interface parameters such as the contact pressure and the surface velocity.

Consequently, the value of the friction coefficient depends on the amount of lubricant present between the two surfaces. Upon comparing the film thickness (h) and the rough mean square (R.M.S) (R_q) of the surface roughness, we can distinguish three lubrication regimens:

- The hydrodynamic lubrication regimen when $h \geq 3R_q$: This regimen is characterized by a very low friction coefficient. The surfaces are completely separated by the film of lubricant, which prevents any metal/metal contact. The load is completely carried by the lubricant. In the hydrodynamic regimen, two subregimens can be said to exist: a fully hydrodynamic one (FHL) where $h \geq 10R_q$, and an elastohydrodynamic one (EHL) where $3R_q \leq h < 10R_q$. In EHL lubrication, even if contact does not occur, the roughness affects the lubricant flow.
- The boundary lubrication regimen (BL) when $h \leq R_q$: In this case, physical contact occurs between the interacting surfaces, and the load is carried entirely by the surface roughness peaks which are in physical contact with each other. This regimen is characterized by a very high friction coefficient, which results from complex surface interactions: the shearing of asperities, chemical interactions, etc.
- The mixed lubrication regimen (ML) where $R_q < h < 3R_q$: This is the regimen in between the hydrodynamic and boundary ones. The load on the interface is partly carried by the lubricant and partly by the interactions between metal surfaces. In this case, the following two phenomena are mainly involved:
  - Dry friction at the effective contact part of the surface,
  - EH lubrication in the valley.

The mixed regimen, therefore, has to be studied at the asperity scale, whereas the hydrodynamic and

Table 2
Material properties of the coining process

Dimensions	Length = 8 mm Width = 3 mm Tool length = 4 mm
Material properties	E = 210,000 MPa $\mu = 0.3$ $A_0(\bar{\varepsilon}_p) = 250 + 10000\bar{\varepsilon}_p$

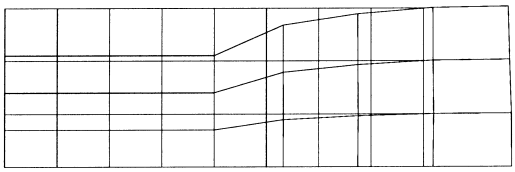

Fig. 5. Deformed mesh in ALE formulation.

boundary ones can be studied on the workpiece scale (see, for example, Hu et al., 1994; Wilson and Marsault, 1998; Wilson and Wang, 1984).

6.1. Modeling the flow in hydrodynamic and elastohydrodynamic lubrication

The following assumptions were made to render the analysis tractable:

- The lubricant is Newtonian with constant viscosity η.
- The fluid flow is laminar.
- The lubricant is incompressible.
- The surfaces are smooth.
- Thin film hypothesis: the film thickness h is small in comparison with the length of the lubricated zone.

Under these assumptions, the classical Naviers–Stokes equations lead to the Reynolds equation used to describe thin film flows, which is written here for the 2D-case:

$$\frac{\partial}{\partial x}\left(\frac{h^3}{12\eta}\frac{\partial P}{\partial x}\right) = \frac{\partial h}{\partial t} + \frac{\partial (hU_x)}{\partial x} \tag{31}$$

This equation gives the film thickness h depending on the pressure in the lubricant P, the velocities of the two surfaces (with U_x the sum of the surface velocities: $U_x = (1/2)(U_a + U_b)$) and the lubricant

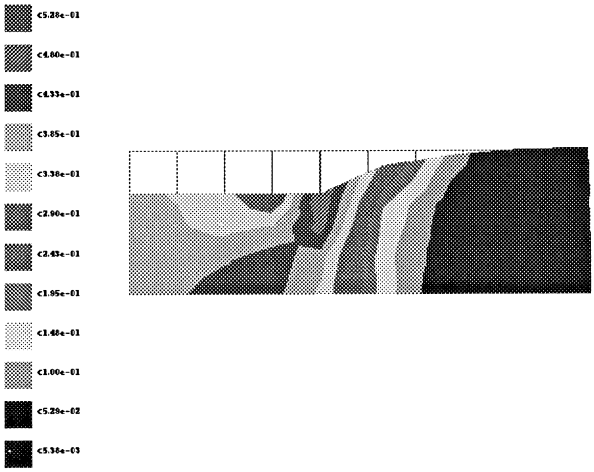

Fig. 6. $\bar{\varepsilon}_p$ with C_0 remapping.

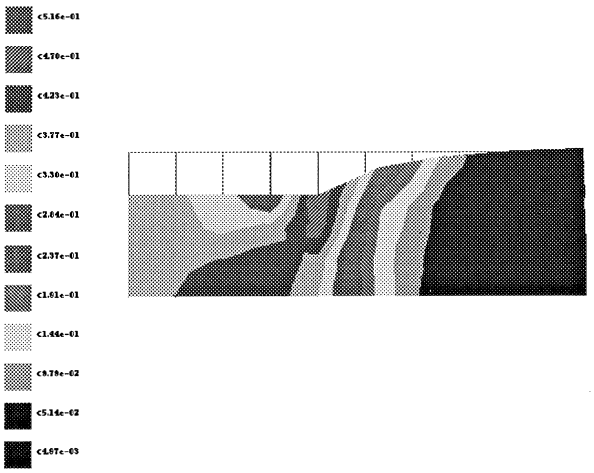

Fig. 7. $\bar{\varepsilon}_p$ with C_t remapping.

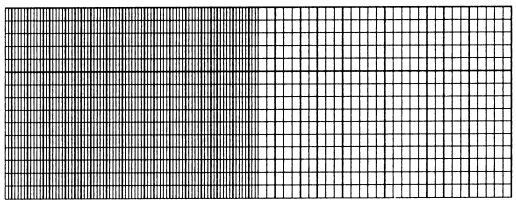

Fig. 8. Initial mesh for Lagrangian calculation.

viscosity η. This equation is fairly effective in lubrication processes between smooth surfaces or when the asperities do not affect the flow, as in the completely hydrodynamic regimen. In order to account for the surface roughness (EHL regimen), an average Reynolds equation developed by Patir and Cheng (1978) is used:

$$\frac{\partial}{\partial x}\left(\Phi_x \frac{h_m^3}{12\eta}\frac{\partial \bar{P}}{\partial x}\right) = \frac{\partial h}{\partial t} + \frac{\partial (h_m U_x)}{\partial x} + \frac{1}{2}\frac{\partial \left(V_x R_q \Phi_s\right)}{\partial x} \tag{32}$$

where h_m is the film thickness between the mean surfaces and the real film thickness is given by $h = h_m + \delta_a + \delta_b$, where δ_a (resp. δ_b) is the amplitude of the surface roughness a (resp. b) (see Fig. 10). V_x is the relative surface velocity $V_x = U_a - U_b$ and $\bar{P}$ the average pressure between the mean surfaces.

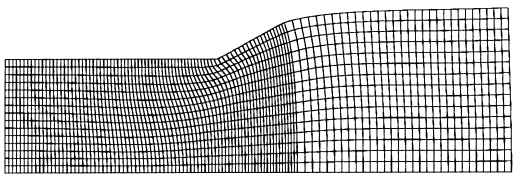

Fig. 9. Deformed mesh for Lagrangian calculation.

The effects of the surface roughness are dealt with by introducing Φ_x, and Φ_s, which are flow factors depending on the film thickness h and on the asperity geometries via R_q and the Peklenik number γ. Φ_x is the pressure flow factor which characterizes the mean presure flow in the rough case, based on that determined in the smooth case with the same nominal geometry.

$$\Phi_x = 1 - Ce^{-rH} \text{ pour } \gamma \leq 1$$

$$\Phi_x = 1 - CH^{-r} \text{ pour } \gamma > 1 \tag{33}$$

Coefficients C and r depend on γ and $H = h/R_q$. Elastohydrodynamic lubrication with isotropic roughness leads to:

$$H > 0.5, \quad \gamma = 1 \Longrightarrow C = 0.9 \quad \text{and} \quad r = 0.56$$

In Eq. (32), $\partial(V_x R_q \Phi_s)/\partial x$ is an additional term due to the combined effects of roughness and sliding. The shear flow factor Φ_s is a function of parameters depending on each of the surfaces:

$$\Phi_s = \left(\frac{R_q^a}{R_q}\right)^2 \phi\left(H, \gamma^a\right) - \left(\frac{R_q^b}{R_q}\right)^2 \phi\left(H, \gamma^b\right) \tag{34}$$

R_q^i is the R.M.S associated with the surface i and R_q the combined one, ϕ is a positive function of H, and γ^i the Peclenik number associated with surface i:

$$\phi = A_1 H^{\alpha_1} e^{-\alpha_2 H + \alpha_3 H^2} \quad \text{for } H \leq 5$$

$$\phi = A_2 e^{-0.25H} \quad \text{for } H > 5 \tag{35}$$

In elastohydrodynamic lubrication with isotropic roughness, coefficients A_1, A_2, A_3, α_1, α_2 and α_3 are given by:

$$A_1 = 1.899,\ A_2 = 1.126,\ \alpha_1 = 0.98,\ \alpha_2 = 0.92 \text{ and } \alpha_3 = 0.05$$

Although the Patir and Cheng model is the most commonly used model, various flow factor expressions have also been established by other authors (see, for example, Peeken et al., 1997; Tripp, 1983).

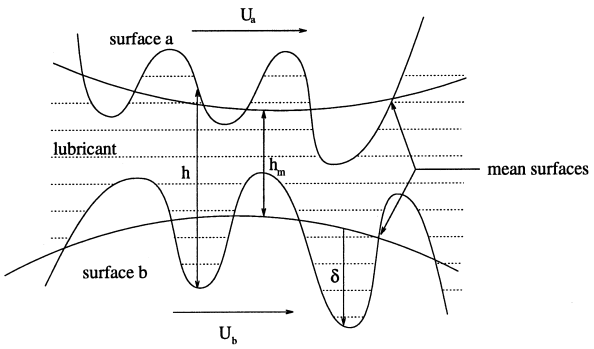

Fig. 10. Schematic surface roughness.

Comment. In hydrodynamic lubrication, the average Reynolds equation leads to the smooth case equation with:

$$H = \frac{h}{R_q} \to \infty \quad \Phi_x \to 1 \quad \Phi_s \to 0.$$

6.2. Determination of film thickness

Wilson (see, for example, Wilson and Wang, 1984) has divided the lubricated domain into three zones: an inlet zone, a work zone and an outlet zone (as presented schematically in Fig. 11). The amount of lubricant which will be entrained into the work zone depends on the film thickness h_B at the boundary between the inlet and work zones (point B).

6.2.1. Inlet zone analysis

In the inlet zone, the pressure depends on the lubricant hydrodynamics and increases from the atmospheric value to a maximum at the boundary between the inlet and work zones. The surfaces are rigid and the tools do not affect the lubricant flow. Their geometries do, however, affect the shape of the film lubricant in the neighbourhood of point B. The problem is set as a quasi-steady one and the average 2D Reynolds equation (32) is written:

$$\frac{\mathrm{d}}{\mathrm{d}x}\left(\Phi_x \frac{h_m^3}{12\eta}\frac{\mathrm{d}P}{\mathrm{d}x}\right) = \frac{\mathrm{d}(h_m U_x)}{\mathrm{d}x} \tag{36}$$

Assuming the pressure, pressure gradient, velocity and pressure flow factor to remain constant keeping the values reached at the boundary between the inlet and work zones, the film thickness h_m^B is determined by:

$$2\Phi_x^B \bar{P}_B h_m^B tg\alpha + 12\eta U_x^B + \Phi_x^B h_m^{B^2} \bar{P}'_B = 0 \tag{37}$$

This second degree equation is solved, given the film thickness h_m^B:

$$h_m^B = \frac{-\bar{P}_B tg\alpha \Phi_x^B + \sqrt{\Delta}}{\bar{P}'_B \Phi_x^B} \tag{38}$$

where $\Delta = (\bar{P}_B tg\alpha \Phi_x^B)^2 - 12\eta U_x^B \bar{P}'_B \Phi_x^B$.

6.2.2. Work zone analysis

Under the tool, the domain occupied by the lubricant is called the work zone. In the Reynolds equation (32), the gradient of the Poiseuille term: $(h_m^3/\eta)(\partial P/\partial x)$ is negligible in comparison with the gradient of the Couette term: $h_m U_x$ (see, for example, Lugt et al., 1993; Wilson and Wang, 1984). In addition, the velocity and pressure along the contact interface vary slowly in comparison with the film thickness. The partial derivative equation to be solved is then as follows:

$$12\frac{\partial h_m}{\partial t} + 6\frac{\partial}{\partial x}(h_m U_x) + 6\frac{\partial\left(V_x R_q \Phi_s\right)}{\partial x} = 0 \tag{39}$$

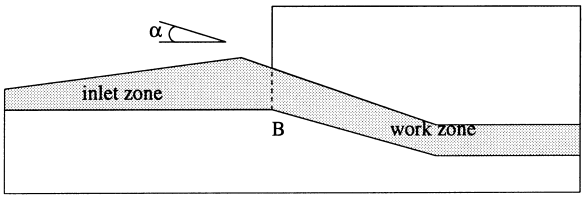

Fig. 11. Inlet and work zones.

Eq. (39) is a hyperbolic equation which can be solved using a characteristic method. Along the curve defined by:

$$\frac{\mathrm{d}x}{\mathrm{d}t} = \frac{1}{2}U_x \tag{40}$$

the Eq. (39) takes the form:

$$\frac{\mathrm{d}h_m}{\mathrm{d}t} = Ch_m + D \tag{41}$$

where $C = -(1/2)(\partial U_x/\partial x)$ and $D = -(1/2)(\partial(V_x R_q \Phi_s)/\partial x)$. An analytical integration of Eq. (41) gives:

$$h_m = \frac{\left(Ch^0 + D\right)\mathrm{e}^{C(t-t^0)} - D}{C} \tag{42}$$

At time t^0, the initial condition h_m^0 is given by the inlet zone analysis (i.e. $h_m^0 = h_m^B$).

Once the film thickness has been determined, it is necessary to compare h_m with R_q in order to characterize the lubrication regimen:

- If $h_m \geq 10R_q$, this is the completely hydrodynamic regimen. The friction corresponds to the shearing in the lubricant film. The friction coefficient is determined using the ratio between the shear stress τ and the pressure P:

$$\tau = \eta\frac{V_x}{h_m} + \frac{h_m}{2}\frac{\partial P}{\partial x} \tag{43}$$

- If $3R_q \leq h_m \leq 10R_q$, this is the EH regimen. In order to account for the surface roughness, we use corrector terms in the expression for the shear stress in the lubricant film determined by Patir and Cheng (1978, 1979):

$$\tau = \eta\frac{V_x}{h_m}\left(\Phi_f + \Phi_{fs}\right) + \frac{h_m}{2}\Phi_{fp}\frac{\partial \bar{P}}{\partial x} \tag{44}$$

where Φ_{fp} is the corrector factor for the mean pressure flow component. Its expression has the same form as Φ_x in the average Reynolds equation:

$$\Phi_{fp} = 1 - D\mathrm{e}^{-sH}$$

Coefficients D and s depend on the Peklenick number γ and if the roughness is isotropic, their values are:

$$D = 1.40 \quad \text{and} \quad s = 0.66$$

Φ_{fs}, like Φ_s in the average Reynolds equation, arises from the combined effects of the roughness and sliding:

$$\Phi_{fs} = \left(\frac{R_q^a}{R_q}\right)^2 \phi_{fs}(H, \gamma^a) - \left(\frac{R_q^b}{R_q}\right)^2 \phi_{fs}(H, \gamma^b)$$

with

$$\phi_{fs} = \begin{cases} A_3 H^{\alpha_4} e^{-\alpha_5 H + \alpha_6 H^2} & H < 7 \\ 0 & H \geq 7 \end{cases}$$

Here, we use:

$$A_3 = 11.1,\ \alpha_4 = 2.31,\ \alpha_5 = 2.38 \text{ and } \alpha_6 = 0.11$$

The expression for ϕ_f, which is the average value of the shear stress sliding velocity component, is given by:

$$\Phi_f = \frac{35}{32} z \left\{ (1 - z^2) \ln \frac{z+1}{z-1} + \frac{z}{15}\left[66 + z^2(30z^2 - 80)\right] \right\} \quad H > 3$$

$$\Phi_f = \frac{7}{6} \quad H = 3$$

where $z = H/3$.

- If $h_m < 3R_q$, a Coulomb constant friction coefficient is used. This constitutes a considerable simplification of the phenomema occurring in mixed and boundary regimens. Although the boundary regimen can be modeled by a constant friction coefficient, the asperity scale must be studied to account for the mixed regimen. We decided to study the workpiece scale in order to describe the metal forming process.

6.3. Numerical implementation

The lubrication was analyzed with the characteristic computational process based on Eulerian formulation, while the workpiece plasticity was analyzed based on Lagrangian formulation, assuming that at time t_{i-1}, Eqs. (40) and (41) are integrated from the material node (grid node). At time t_i, the end point of the characteristic method solution does not coincide with the same node (see Fig. 12). Some of the variables (pressure and velocity) necessary for determining the shear stress τ are known at the mesh nodes, whereas the film thickness h is known at the end of the characteristic method computational process.

In order to overcome this problem, Chen and Sun (1986) have proposed an interpolation. Here, we use the ALE formulation presented above. After the Lagragian step corresponding to the integration of Eqs. (40) and (41) and after some structural computation, the Eulerian step is started by remeshing the structure.

- In the inlet zone, the lubricant does not affect the deformation of the structure, and therefore, there is no remeshing of nodes in this zone.

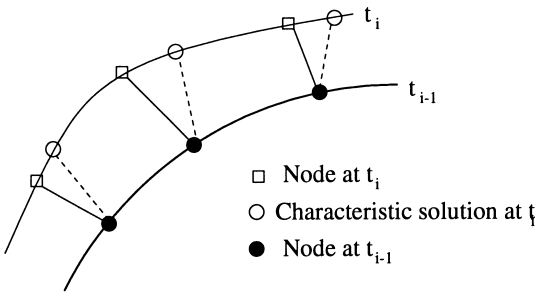

Fig. 12. Paths of characteristic and F.E. nodes.

- The work zone is treated like an ALE macroregion. Before computing the shear stress τ, the remeshing step relocates the mesh nodes on the contact interface (in 2D the contact interface constitutes a master line) at the position of the end points of the characteristic computational process. The transfinite mapping method is used to generate the internal mesh.

The second part of the Eulerian step consists of transporting the values onto the new mesh. Here, we use the remapping algorithm on the initial configuration presented above. The plasticity and lubrication analyses are linked together at each step in the incremental computation as shown:

- Start of incremental step:
  1. Solid part of calculation:
     – Determining lubricated zones.
     – Computing nodal pressure and velocities.
  2. Fluid part of calculation:
     – Inlet zone analysis: computing the boundary film thickness h_m^B.
     – Work zone analysis: computing the nodal film thickness h_m.
  3. ALE part of calculation:
     – Remeshing phase: node location is equal to characteristic end point location.
     – Transporting value onto the new mesh (structure and fluid steps results)
  4. Nodal friction coefficient calculation:
     – Characterizing the lubrication regimen.
     – Computating the shear stress and friction coefficient μ.
- If convergence is achieved, start the next increment, or go back to (1) with the new friction coefficient.

7. Numerical examples

7.1. Punch stretch forming test

The first example is a numerical simulation of hemispherical punch stretch forming proposed by Woo (1993). Fig. 13, gives the geometry of the workpiece and tools. The dimensions and material properties are described in Table 3.

A 180 elements axisymmetric mesh is used and the work zone under the punch constitutes the

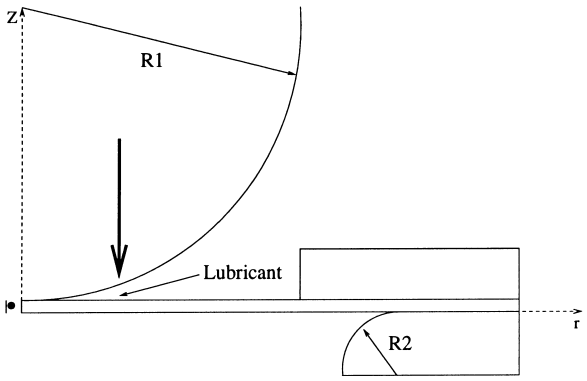

Fig. 13. Geometry of punch stretch forming.

remeshed zone according to the characteristic method. The lubricant under the punch is taken to have a viscosity $\eta = 0.445$ Pa s, and the R.M.S of the workpiece is equal to 0.4 μm. The punch is assumed to be a rigid, smooth tool, and assumed to move vertically 33 mm.

Fig. 14 shows the deformed mesh at the end of the process. The thinning of the workpiece visible on the deformed mesh can be seen along the contact zone in Fig. 15, and the maximum is reached at the center of the sheet, as previously reported by Dubois (1994), based on the low friction coefficient.

The film thickness evolves in parallel with the deformation of the workpiece. In Fig. 16 and 17, the film thickness is maximum at the center of the sheet. This leads to a hydrodynamic regimen and a very

Table 3
Dimensions and material properties

Dimensions	Length = 56.38 mm
	Thickness = 0.89 mm
	Punch radius, $R1$ = 25.4 mm
	Drawbead radius, $R2$ = 12.7 mm
Material properties	E = 69,004 MPa
	$\mu = 0.3$
	$A_0(\bar{\varepsilon}_p) = 589(10^{-04} + \bar{\varepsilon}_p)^{0.216}$

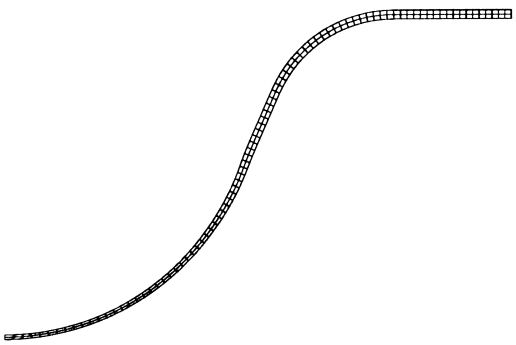

Fig. 14. Deformed mesh.

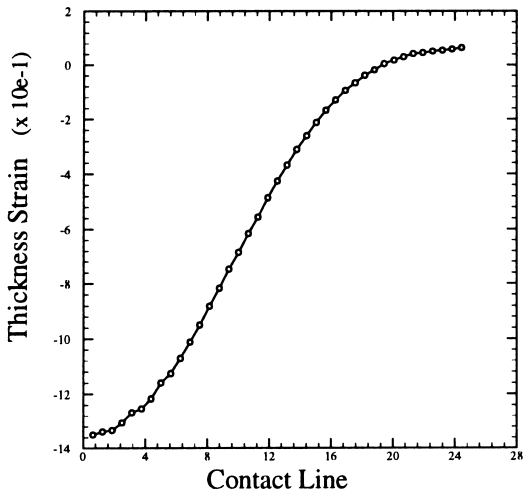

Fig. 15. Thickness strain along contact zone.

low friction coefficient. Along the contact zone, h decreases and friction coefficient μ therefore increases. Since the mixed regimen is given by a constant friction coefficient, this leads to the discontinuity visible in Fig. 17.

7.2. Flat die test

The second example given in Fig. 18 is a classical tribological test with flat dies. It consists of two steps: the sheet is clamped in order to obtain a clamping force of 50 N. In the second step, the sheet is being drawn with a constant velocity of 16 mm s^{-1}, keeping the clamping force constant. The dimensions and mechanical characteristics are presented in Table 4. The lubricant used has a high viscosity of $\eta = 6$ Pa s and the R.M.S of the sheet is 2.5 μm. The main difficulty arising in this test is

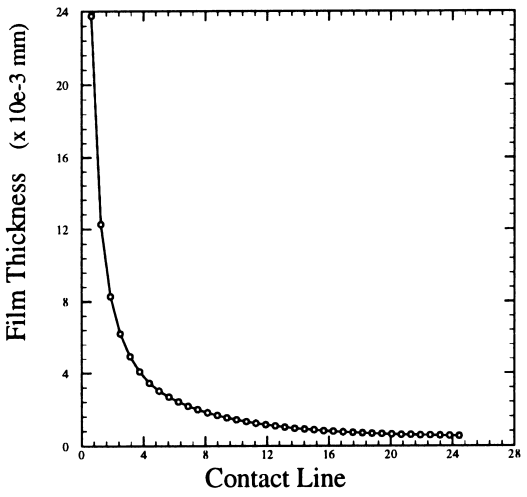

Fig. 16. Film thickness along the contact zone.

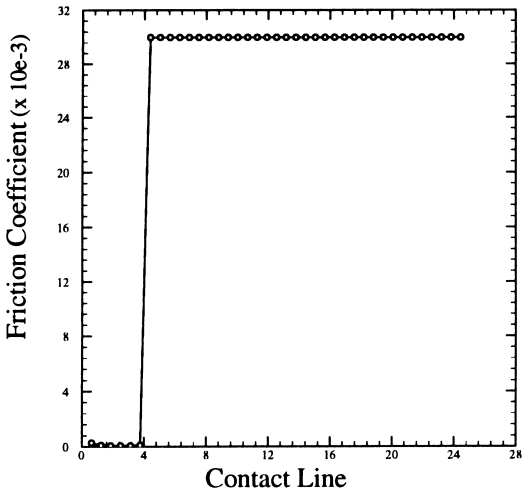

Fig. 17. Friction coefficient along the contact zone.

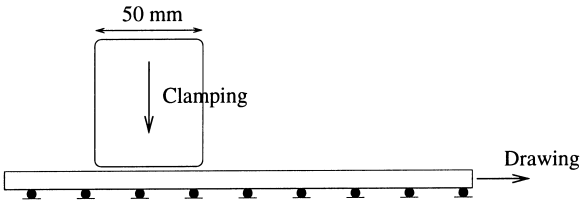

Fig. 18. Geometry of punch stretch forming.

Table 4
Dimensions and material properties

Dimensions	Length = 170 mm Thickness = 0.79 mm Tool length = 50 mm
Material properties	E = 70,000 MPa $\mu = 0.35$ $A_0(\bar{\varepsilon}_p) = 540(0.00805 + \bar{\varepsilon}_p)^{0.28}$

shown in Fig. 19. The global friction coefficient is presented for various drawing values, and two cases are studied:

- Completely hydrodynamic regimen given here by a classical Reynolds equation.
- Elastohydrodynamic regimen given here by an average Reynolds equation.

As we can see, after an accomodation step, the friction coefficient oscillates, reflecting a stick-slip phenomenon.

The contact pressure and velocity are given in Figs. 20 and 21 during one oscillation. The real contact area (where the presssure is maximum and the velocity equal to zero) decrease during the drawing

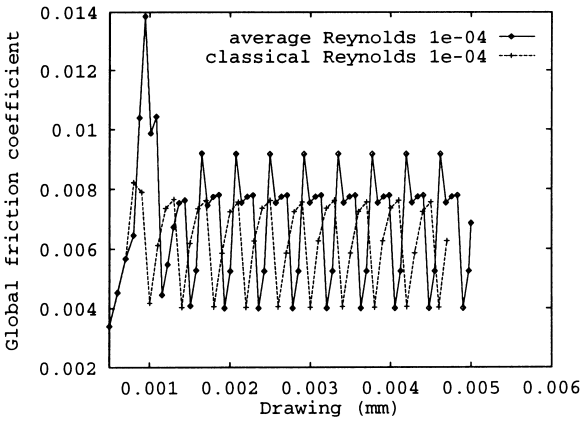

Fig. 19. Global friction coefficient.

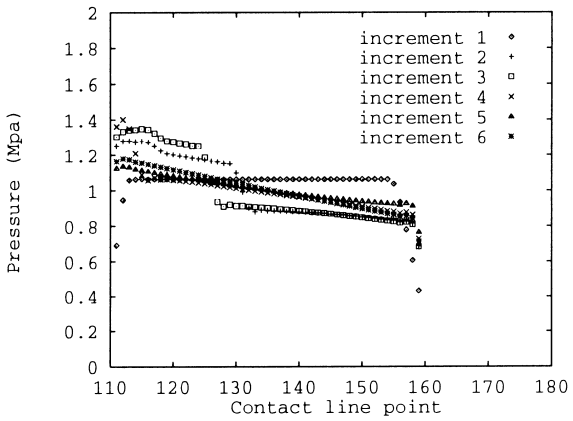

Fig. 20. Pressure along the contact zone.

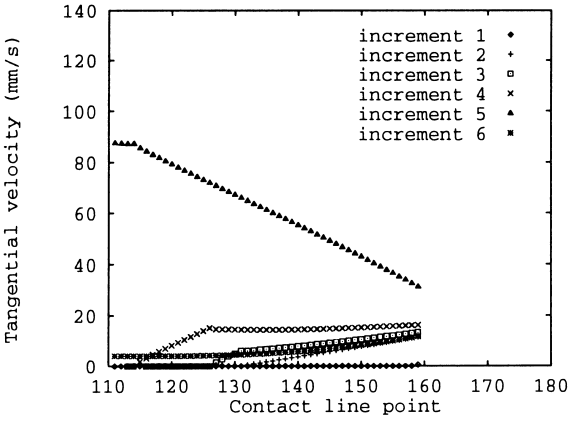

Fig. 21. Velocity along the contact zone.

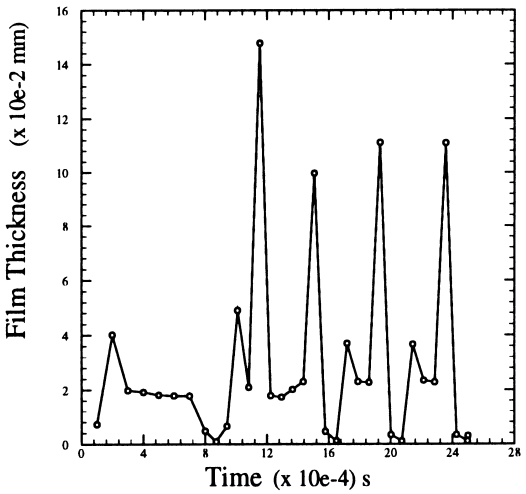

Fig. 22. Film thickness during drawing.

process: increments 1–4. When sliding occurs (increment 5), the velocity is larger at every node along the contact zone than the prescribed one and the pressure is restored along the contact zone. Since the clamping force is constant and the friction dissipation is too low to prevent the initial sheet thickness from being recovered, the workpiece is in the same state at increment 6 as at increment 1.

Locally, the friction coefficient of one node in the contact zone differs from the hydrodynamic value $\mu = 0.002$ and the boundary one $\mu = 0.18$. Since the mixed regimen is given by a constant friction coefficient, this leads to a discontinuity in the friction coefficient (Figs. 22 and 23).

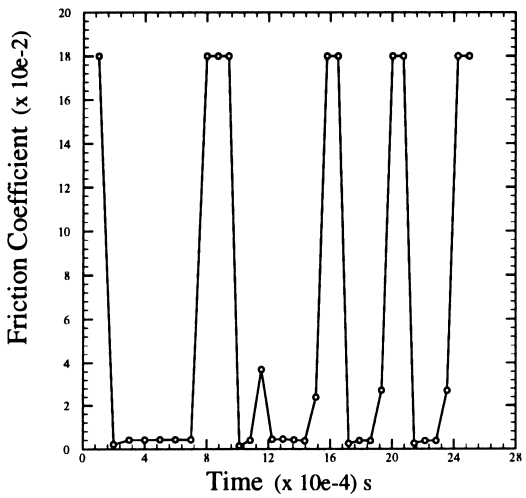

Fig. 23. Friction ceofficient during drawing.

8. Conclusion

In the present study, a new application of ALE formulation to fluid/structure coupling problems is described. This system of formulation was originally developed in Lagrangian terms for studying the contact with friction problems arising in metal working processes, and had to be adapted here to the existing elastoplastic model.

After accounting completely for the large deformation problem using a hyperelastic behavioral law, the ALE formulation was applied to a solid mechanics problem and found to have advantages over the classical Lagrangian scheme of formulation; since the simple meshing used is not deformed, no time-consuming refinement steps are required.

By modeling the lubricant at the interface, it was possible to establish a local friction coefficient depending on the roughness of the metal sheet, the thickness of the film and the pressure and velocity of the two surfaces involved in the friction. With our numerical model a stick–slip phenomenon was detected during the plane-to-plane testing.

The scale of the structure was taken to be the only factor limiting the study of the mixed regimens and that of the boundary regimens to a constant friction coefficient.

References

Belytschko, T., Kennedy, J.M., 1978. Computer models for subassembly simulation. Nucl. Engrg. Des 49, 17–38.

Benson, D.J., 1989. An efficient, accurate, simple ALE method for nonlinear finite element programs. Comput. Methods Appl. Mech. Engrg 72, 305–350.

Carleer, B., 1997. Finite element analysis of deep drawing. Ph.D. Thesis, University of Twente, Netherlands.

Chabrand, P., Chertier, O., 1996. Variable friction coefficient model in deep drawing. In: Proceedings of the 5th ICTP, Colombus, Ohio.

Chabrand, P., Chertier, O., Dubois, F., Martinet, F., 1998. Variable friction coefficient model in sheet metal forming. In: Huétink, J., Baaijens, F. (Eds.), Numiform'98, Simulation of Materials Proceessing: Theory, Methods and Applications. Balkema, pp. 845–850.

Chen, K., Sun, D., 1986. Hydrodynamic lubrication in hemispherical punch stretch forming. ASME J 53, 440–449.

Donéa, J. 1978. Finite element analysis of transient dynamic fluid-stucture interaction. In: Donéa, J. (Ed.), Advanced Structural Dynamics. Advance, London, UK, pp. 255–290.

Donéa, J., Giuliani, S., Halleux, J., 1982. An arbitrary Lagrangian–Eulerian FEM for transient dynamic fluid-structure interactions. Comput. Methods Engrg 33, 689–723.

Dubois, F., 1994. Contact, frottement, grandes déformations élastoplastiques. Application á l'emboutissage. Ph.D. Thesis, Université de la Méditérranée.

Gaston, L., Bellet, M., Chenot, J., 1996. An ALE finite element approach to non steady state fluid flows. Application to mould filling. In: Numerical Methods in Engineering'96.

Haber, R., Shepard, Abel, Gallagher, Greenberg, 1981. A general, two dimensional, graphical finite element preprocessor utilizing discrete transfinite mappings. Int. J. Numer. Methods Engrg. 17, 1015–1044.

Hinton, E., Campbell, L., 1974. Local and global smoothing of discontinuous finite element functions using a least square method. Int. J. Numer. Methods Engrg. 8, 461–480.

Hu, Y., Cheng, H.S., Arai, T., Kobayashi, Y., Aoyama, S., 1994. Numerical simulation of piston ring in mixed lubrication —a nonaxisymmetrical analysis. ASME J. of tribology 116, 470–478.

Huetink, J., van der Lugt, J., 1990. Progress in mixed Eulerian–Lagrangian finite element simulation of forming process. Int. J. for Num. Meth. Engng 30, 1441–1457.

Hugues, T.J.R., Liu, W.K., Zimmerman, T.K., 1981. Lagrangian–Eulerian FE formulation for incompressible viscous flows. Comput. Methods Appl. Mech. Engrg 29, 329–349.

Ike, H., Makinouchi, A., 1990. Effect of lateral tension and compression on plane strain flattening asperities lying over a plastically deformable bulk. Wear 140, 17–38.

Lee, E.H., 1969. Elastic–plastic deformation at finite strains. J. Appl. Mech. Engrg 36, 1–6.

Liu, W.K., Belytschko, T., Chang, H., 1986. An arbitrary Lagrangian–Eulerian finite element method for path-dependent materials. Comput. Methods Appl. Mech. Engrg 58, 227–245.

Liu, W.K., Chang, H., Chen, J.S., Belytschko, T., 1988. Arbitrary Lagrangian–Eulerian Petrov–Galerkin finite element for non linear continua. Comput. Methods Appl. Mech. Engrg 68, 259–310.

Lugt, P.M., Wemekamp, A.W., ten Napel, W.E., 1993. Lubrification in cold rolling: elasto–plasto-hydrodynamic lubrication of smooth surfaces. ASME Wear 166, 203–214.

Patir, N., Cheng, H.S., 1978. An average flow model for determining effects of three-dimensional roughness on partial hydrodynamic lubrication. ASME J., Lu., Tech 100, 12–17.

Patir, N., Cheng, H.S., 1979. Application of average flow model to lubrication between rough sliding surfaces. ASME J., Lu., Tech 101, 220–230.

Peeken, H.J., Koll, G., Rienacker, A., Lang, J., Schonen, R., 1997. On numerical determination of flow factors. ASME J. of tribology 119, 259–264.

Ponthot, J., 1995. A finite element unified treatment of continuum mechanics for solids submitted to large strains. Ph.D. Thesis, Université de Liège, Belgium.

Potapov, S., Jacquart, G., 1996. A new ALE algorithm based on a mixed finite element-finite volume approach. In: Numerical Methods in Engineering'96.

Scheurs, P.G.J., Veldpaus, F.E., Brekelmans, W.A.M., 1986. Simulation of forming processes using the Arbitrary Eulerian Lagrangian formulation. Comput. Methods Appl. Mech. Engrg 58, 19–36.

Sidoroff, F., 1982. Incremental constitutive equation for large strain elastoplasticity. Int. J. Eng. Sci 20, 19–26.

Simo, J.C., Miehe, C., 1992. Associative coupled thermoplasticity at finite strains: formulation, numerical analysis and implementation. Comput. Methods Appl. Mech. Engrg 98, 41–104.

Tripp, J.H., 1983. Surface roughness effects in hydrodynamic lubrication: the flow factor method. ASME J. of lubrication technology 105, 458–465.

Wilson, W.R.D., Marsault, N., 1998. Partial hydrodynamic lubrication with large fractional contact areas. ASME J. of tribology 120, 1–5.

Wilson, W., Sheu, S., 1988. Real area of contact and boundary friction in metal forming. Int. J. Mech. Sci 30, 475–489.

Wilson, W.R.D., Wang, J.J., 1984. Hydrodynamic lubrication in simple stretch forming processes. ASME J. of tribology 106, 70–77.

Woo, D.M., 1993. On complete solution of deep drawing problem. Int. J. Mech. Sci 10, 83–94.

Yamada, T., Kikuchi, F., 1993. An arbitrary Lagrangian–Eulerian finite element method for incompressible hyperelasticity. Comput. Methods Appl. Mech. Engrg 102, 149–177.